International Journal of Coal Geology 253 (2022) 103970

Contents lists available at ScienceDirect

International Journal of Coal Geology

journal homepage: www.elsevier.com/locate/coal

Origin of organic matter and organic pores in the overmature Ordovician-Silurian Wufeng-Longmaxi Shale of the Sichuan Basin, China

Juan Teng [a], Bei Liu [b,c,*], Maria Mastalerz [d], Juergen Schieber [c]

[a] College of Resources and Environment, Yangtze University, Wuhan, Hubei 430100, China
[b] Key Laboratory of Tectonics and Petroleum Resources of Ministry of Education, China University of Geosciences, Wuhan, Hubei 430074, China
[c] Department of Earth and Atmospheric Sciences, Indiana University, Bloomington, IN 47405, USA
[d] Indiana Geological and Water Survey, Indiana University, Bloomington, IN 47405-2208, USA

ARTICLE INFO

Keywords:
Organic matter
Maceral
Organic pores
Pyrobitumen
Graptolite
Vitrinite-like particle
Acritarchs
Wufeng-Longmaxi Shale

ABSTRACT

Organic matter (OM)-hosted pores play important roles in controlling the porosity and gas content of gas shales. However, the control of organic pore development and preservation remains poorly understood, partly because of the inability to distinguish OM types under the scanning electron microscope (SEM). In this study, seven overmature Wufeng-Longmaxi Shale samples (equivalent vitrinite reflectance 1.93%–3.07%) were investigated with organic petrography and scanning electron microscope to study the origin of OM and development of organic pores in this black shale succession. Correlative light and electron microscopy was employed to examine pore development in individual macerals. Organic petrographic observations show that OM in these over-mature black shales is dominated by pyrobitumen and graptolites (> 90 vol% of total OM based on point counting). Pyrobitumen mainly occurs as matrix bitumen in the fine-grained matrix, and also as a mixture with clay minerals and fossil cavity infillings. Vitrinite-like particles are minor constituents of OM in the Wufeng-Longmaxi Shale, and their average reflectance, reflectance distribution, and morphology suggest that they may be derived from graptolite fragments lacking diagnostic features and acritarchs. OM type critically controls the development of organic pores. Organic pores primarily occur in pyrobitumen, whereas other macerals are mostly non-porous when examined under the SEM. Results of this study provided important insights into OM thermal evolution and organic pore development in source-rock reservoirs, calling for a critical appraisal of OM in black shales with organic petrography in addition to SEM.

1. Introduction

Organic matter (OM) in organic-rich sedimentary rocks, such as black shales and coals, is the source of oil and gas (Tissot and Welte, 1984). Its quantity, quality, and thermal maturity determine the hydrocarbon generation potential of petroleum source rocks (Tissot and Welte, 1984; Suárez-Ruiz et al., 2012; Hackley and Cardott, 2016; Mastalerz et al., 2018; Hackley et al., 2021). OM-hosted pores are an important component of the pore system of tight shale reservoirs (Loucks et al., 2009, 2012; Schieber, 2010; Katz and Arango, 2018; Mastalerz et al., 2018; Chen et al., 2021; Liu et al., 2021, 2022). Documenting OM type and its control on the development of OM-hosted pores in black shales is of great importance for conventional source rock evaluation and unconventional reservoir characterization.

Dispersed OM in black shales consists of five maceral groups, with each group containing multiple macerals (Potter et al., 1998; Stasiuk et al., 2002; Hackley and Cardott, 2016; Flores and Suárez-Ruiz, 2017; Mastalerz et al., 2018; Liu et al., 2022). Common macerals in black shales are amorphous organic matter (also named bituminite; Teichmüller and Ottenjann, 1977), alginite, liptodetrinite, solid bitumen/pyrobitumen, vitrinite, inertinite, and zooclasts (Mastalerz et al., 2018). Amorphous organic matter, alginite, and liptodetrinite are oil-prone macerals, which transform to solid bitumen and hydrocarbons during thermal maturation and do not exist in their original forms after the peak oil window (R_o 0.8–1.0%; Hackley and Cardott, 2016; Liu et al., 2017, 2019, 2022; Mastalerz et al., 2018; Teng et al., 2021). Solid bitumen becomes the dominant OM after the peak oil window (Hackley and Cardott, 2016; Mastalerz et al., 2018; Liu et al., 2019, 2022). In

* Corresponding author at: Key Laboratory of Tectonics and Petroleum Resources of Ministry of Education, China University of Geosciences, Wuhan, Hubei 430074, China.
E-mail address: liubeicugb@outlook.com (B. Liu).

https://doi.org/10.1016/j.coal.2022.103970
Received 14 January 2022; Received in revised form 1 March 2022; Accepted 6 March 2022
Available online 11 March 2022

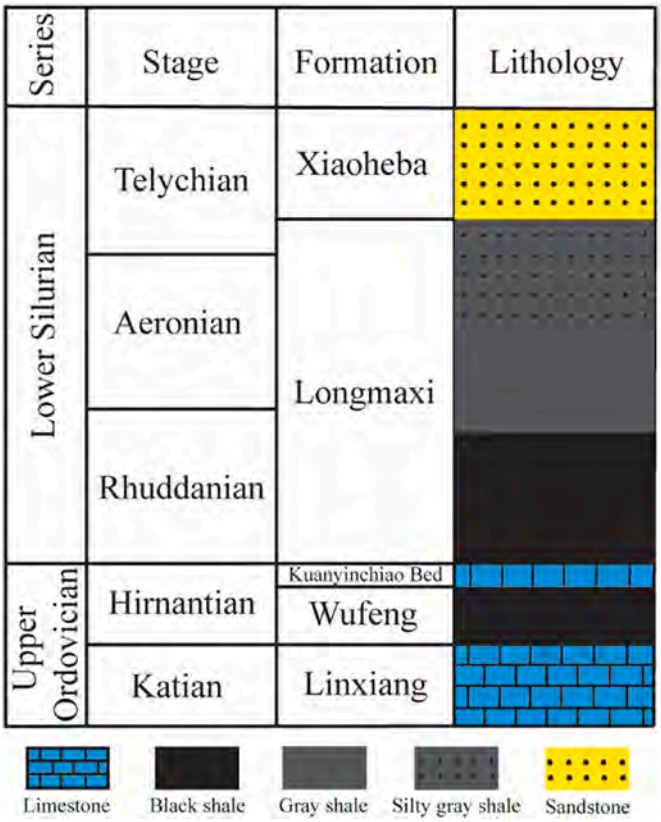

Fig. 1. Chart showing generalized stratigraphy of Upper Ordovician and Lower Silurian in the Sichuan Basin. The thickness of different formations is not to scale.

comparison, vitrinite, inertinite, and zooclasts do not show significant changes in morphology with increasing levels of thermal maturation due to their low hydrocarbon generation potential (Liu et al., 2019, 2022).

OM-hosted pores in black shales include primary and secondary organic pores (Liu et al., 2017, 2022; Katz and Arango, 2018). Primary organic pores are derived from the original biological structure of OM such as cellular pores in inertinite (Liu et al., 2017, 2022; Cardott and Curtis, 2018; Katz and Arango, 2018). They make limited contributions to the pore network of shale reservoirs because they are mostly filled with diagenetic minerals such as quartz and pyrite (Liu et al., 2017, 2022). Secondary organic pores form during oil and gas generation and expulsion and occur in solid bitumen/pyrobitumen (Liu et al., 2017, 2022; Mastalerz et al., 2018). They contribute significantly to the gas content and porosity of mature black shales (Ross and Bustin, 2009; Hao et al., 2013; Qiu et al., 2020).

The Wufeng-Longmaxi Shale is the largest shale gas play in China and one of the largest shale gas plays in the world (Qiu and Zou, 2020; Qiu et al., 2020; Nie et al., 2021; Sun et al., 2021), with production reaching more than 20.0 × 10^9 m^3 in 2020 (Zou and Qiu, 2021). OM types in this black shale succession and their control on organic pore development are not well understood. Organic petrographic studies show that OM in these organic-rich shales consists of graptolite, pyrobitumen, vitrinite-like particles, and acritarchs (e.g., Luo et al., 2016, 2017, 2018; Wang et al., 2019, 2020, 2021; Yang et al., 2020; Wei et al., 2021; Delle Piane et al., 2022; Qiu et al., 2022). Because of the lack of vitrinite in this black shale succession, the reflectance of graptolite and pyrobitumen has been used to assess the thermal maturity of shales (Luo et al., 2017, 2018; Wang et al., 2019, 2020, 2021). Multiple earlier studies have asserted abundant algae in this black shale succession (e.g., Nie et al., 2018; Hu et al., 2020; Zhang et al., 2020a, 2020b). It has, however, been well documented that oil-prone alginite transforms to solid bitumen and hydrocarbons during thermal maturation and does no longer exist in its original form at high maturity (Hackley and Cardott, 2016; Mastalerz et al., 2018; Liu et al., 2019, 2022; Hackley et al., 2021). The purpose of this study is to probe the origin of OM in the Wufeng-Longmaxi Shale. Specific objectives are to 1) examine OM types in the Wufeng-Longmaxi Shale; and 2) analyze the control of OM types on the development of organic pores.

2. Geological setting

The merging of the Yangtze Block and the Cathaysia Block was initiated during the Neoproterozoic (Qiu et al., 2016) and resulted in the formation of a foreland basin on the northwestern Cathaysia Block and southern Yangtze Block (Li et al., 2017). The Ordovician Wufeng Formation and Silurian Longmaxi Formation of the Sichuan Basin were

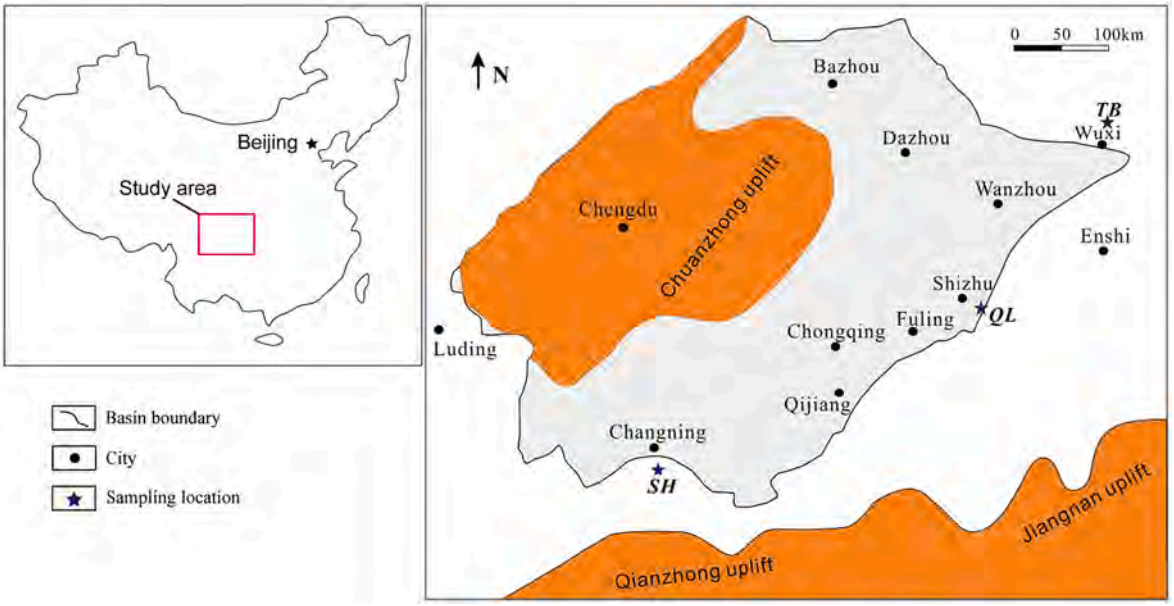

Fig. 2. Map showing the extent of the Sichuan Basin and sampling locations. Modified from Wang et al. (2019). SH = Shuanghe section; QL = Qiliao section; TB = Tianba section.

Table 1
Measured total organic carbon (TOC) content, graptolite reflectance (GR_o), vitrinite-like particle reflectance (VLR_o), pyrobitumen reflectance (BR_o), number of measurements, standard deviation, and calculated equivalent vitrinite reflectance (EqR_o) of the studied shale samples.

Sample	Location	Formation	TOC (wt %)	GR_o	N	SD	VLR_o	N	SD	BR_o	N	SD	EqR_o-1	EqR_o-2
SH-14	Shuanghe section, Changning County, Sichuan	Wufeng Formation	2.12	3.97	89	0.81	3.94	59	0.8	2.52	29	0.39	3.06	2.63
SH-18		Wufeng Formation	2.37	4.01	93	0.80	4.19	58	0.72	2.65	7	0.50	3.09	2.76
QL-06	Qiliao section, Shizhu County, Chongqing	Wufeng Formation	3.95	3.56	81	0.63	3.23	53	0.48	2.27	41	0.30	2.76	2.40
QL-17		Longmaxi Formation	4.27	3.72	132	0.60	3.34	80	0.38	2.47	65	0.39	2.88	2.59
TB-27	Tianba section, Wuxi County, Chongqing	Longmaxi Formation	6.51	2.52	130	0.50	2.21	108	0.36	1.91	39	0.17	2.00	2.05
TB-28		Longmaxi Formation	6.85	2.34	100	0.36	2.11	107	0.27	1.82	33	0.17	1.87	1.97

EqR_o-1: Calculated EqR_o from GR_o based on $EqR_o = GR_o \times 0.73 + 0.16$ (Petersen et al., 2013).
EqR_o-2: Calculated EqR_o from BR_o based on $EqR_o = BR_o \times 0.9528 + 0.2328$ (Schoenherr et al., 2007).
N = number of measurements; SD = standard deviation.

Table 2
Maceral composition of organic matter in the studied shales based on point counting.

Sample	TOC (wt %)	Maceral composition (vol%, on mineral-matter-free basis)			
		Pyrobitumen	Graptolite	Vitrinite-like particle	Acritarch
SH-14	2.12	75.4	19.2	5.4	–
SH-18	2.37	73.1	20.8	6.1	–
QL-06	3.95	74.9	18.2	6.5	0.4
QL-17	4.27	71.5	20.2	7.5	0.7
TB-27	6.51	69.8	22.6	7.2	0.4
TB-28	6.85	67.0	24.4	8.0	0.6

"–" = not detected.

deposited in the Yangtze Shelf Sea (Zou et al., 2018, 2019). Geographically, the Wufeng-Longmaxi Shale mainly occurs in easter Sichuan, Chongqing, northern Guizhou, and western Hubei. Stratigraphically, it overlies the Linxiang Formation limestone and underlies the Xiaoheba Formation sandstone (Fig. 1). Within this black shale succession, the Kuanyinchiao Bed, a fossiliferous limestone or calcareous shale, overlies the Wufeng Formation and underlies the Longmaxi Formation (Fig. 1), and serves as a marker bed for regional correlation. The Wufeng Formation and bottom Longmaxi Formation mainly consist of black siliceous shales and calcareous shales that are the current target interval for shale gas development. The total organic carbon (TOC) content of this interval typically ranges from 2 to 3 wt% and reaches up to 8 wt% locally (Zou et al., 2019; Qiu et al., 2020). Graptolites are common in this black shale succession (Luo et al., 2016, 2017; Ma et al., 2016; Qiu et al., 2018; Gong et al., 2020). The mean graptolite reflectance of the Wufeng-Longmaxi Shale ranges from 1.2% to 5.0% (Wang et al., 2019), indicating that these rocks are dominantly within the dry gas window.

3. Samples and analytical methods

3.1. Samples

Seven samples from three outcrop sections (Fig. 2) were collected to study OM content, type, thermal maturity, and organic pores in the Wufeng-Longmaxi Shale. Three samples are from the Shuanghe (SH) section, Changning County, Sichuan. Two of the three samples were studied for detailed organic petrographic composition. The other four samples are from the Qiliao (QL) section, Shizhu County, Chongqing, and the Tianba (TB) section, Wuxi County, Chongqing, with two samples from each section. Because OM is the focus of this study, only organic-rich black shales were selected.

3.2. Analytical methods

3.2.1. Total organic carbon content

The TOC contents of shale samples were measured using a LECO elemental analyzer (SC832DR). Powdered samples were pretreated with 10 wt% HCl to remove carbonate minerals. Before TOC analysis, solid residues after acid treatment were freeze dried. Solid residues were analyzed with the LECO elemental analyzer, and the measured TOC contents of the solid residues were converted to the TOC contents of corresponding shale samples.

3.2.2. Organic petrography

Shale samples were crushed into rock chips to pass through a 20-mesh sieve. The chips were made into whole-rock pellets following the standard coal petrography procedures (ASTM, 2015). A Leica DM2500 P microscope linked to a Leica DFC 310 FX digital camera was used to document the petrographic characteristics of macerals such as occurrence, colour, size, and texture. The reflectance of graptolite, pyrobitumen, and vitrinite-like particle (VLP) was measured using a Zeiss Photoscope III reflected-light microscope linked to a TIDAS PMT IV photometric system. More than 50 measurements were taken for graptolite reflectance (GR_o) and VLP reflectance (VLR_o). As many as possible measurements were taken for pyrobitumen reflectance (BR_o) because pyrobitumen is generally very small for measurements. Maceral composition of OM in the studied shales was determined based on point counting, with 500 points counted on OM.

3.2.3. Scanning electron microscopic imaging

A field-emission scanning electron microscope (SEM; FEI Quanta 400 FEG) was used to examine pores in OM. Shale samples were first mechanically polished using successively finer grit (as fine as 1 μm) and then argon ion milled with a Gatan 600 DuoMill at 4 kV and a low incident angle (7.5°) for 2 h (Schieber, 2010, 2013; Schieber et al., 2016; Mastalerz and Schieber, 2017). During SEM imaging, the SEM was operated in low vacuum mode at a working distance of about 10 mm and an accelerating voltage of 15 kV. Energy dispersive X-ray spectroscopy was used to determine the composition of minerals.

Correlative light and electron microscopy (Liu et al., 2017, 2022) was used to determine the type of OM seen under the SEM. First, OM types were identified under the reflected-light microscope before SEM imaging. The petrographic pellets were then cut and mounted to a sample holder for argon ion milling. Ion-milled samples were put under the SEM, and the same fields of view with previously identified OM were located under the SEM to examine the pore development characteristics of specific macerals (Liu et al., 2022).

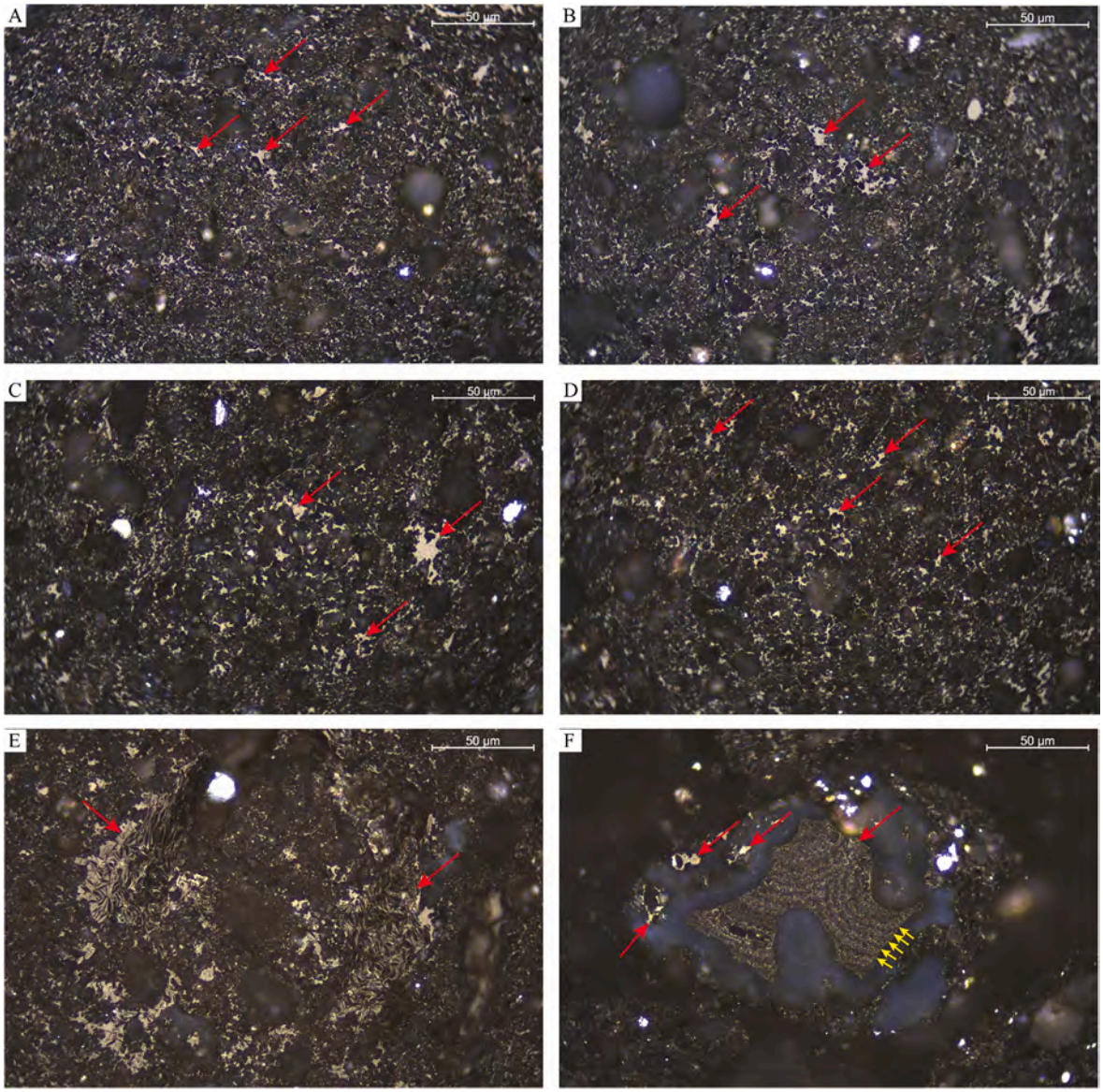

Fig. 3. Photomicrographs of pyrobitumen in reflected white light and oil immersion. (A, B) Pyrobitumen (red arrow), TB-28. (C, D) Pyrobitumen (red arrow), QL-06. Note the fine void-filling wispy nature of pyrobitumen. (E) Pyrobitumen mixed with clay minerals (red arrows) shows distinct patterns, TB-28. (F) Pyrobitumen (red arrow) filling recrystallized radiolarians, SH-14. The radial pattern (yellow arrows) inside the recrystallized radiolarian suggests chalcedonic silica, a typical texture of recrystallized radiolaria (Schieber, 1996). (For interpretation of the references to colour in this figure legend, the reader is referred to the web version of this article.)

4. Results

4.1. Organic matter content and thermal maturity

The TOC content of the studied shale samples ranges from 2.12 to 6.85 wt%, with an average value of 4.35 wt% (Table 1). The average GR_o of the SH, QL, and TB sections is 3.99%, 3.64%, and 2.43%, respectively, which translates into equivalent vitrinite reflectance (EqR_o) of 3.07%, 2.82%, and 1.93%, respectively (Table 1), based on the relationship between GR_o and EqR_o in Petersen et al. (2013). All three sections are in the over-mature stage, with the SH section being the most mature and the TB section the least mature. The EqR_o of the SH, QL, and TB sections calculated from the BR_o based on the relationship between BR_o and EqR_o in Schoenherr et al. (2007) is 2.70%, 2.49%, 2.01%, respectively (Table 1), with the values of the SH and QL sections lower than and the value of the TB section slightly higher than those calculated from the GR_o. The standard deviation of GR_o is higher than that of BR_o for the same sample due to the anisotropy of graptolites. Between samples, higher standard deviation was noticed for high-maturity samples (Table 1).

4.2. Organic matter type

When examined under an optical microscope, OM in the studied shales consists of pyrobitumen, graptolites, VLP, and acritarchs. Pyrobitumen and graptolites are the dominant OM in all three sections, accounting for 72.0 vol% and 20.9 vol% of total OM on average, respectively (Table 2). The contents of VLP and acritarchs are <10 vol% and 1 vol%, respectively. There are no significant changes in maceral composition among the three sections except that no acritarchs were observed in samples from the SH section (Table 2).

Pyrobitumen mainly occurs as fine void-filling wisps (matrix bitumen) and is typically <5 μm (Fig. 3A–D). Pyrobitumen can also be mixed with clay minerals (Fig. 3E) and fill fossil cavities (Fig. 3F).

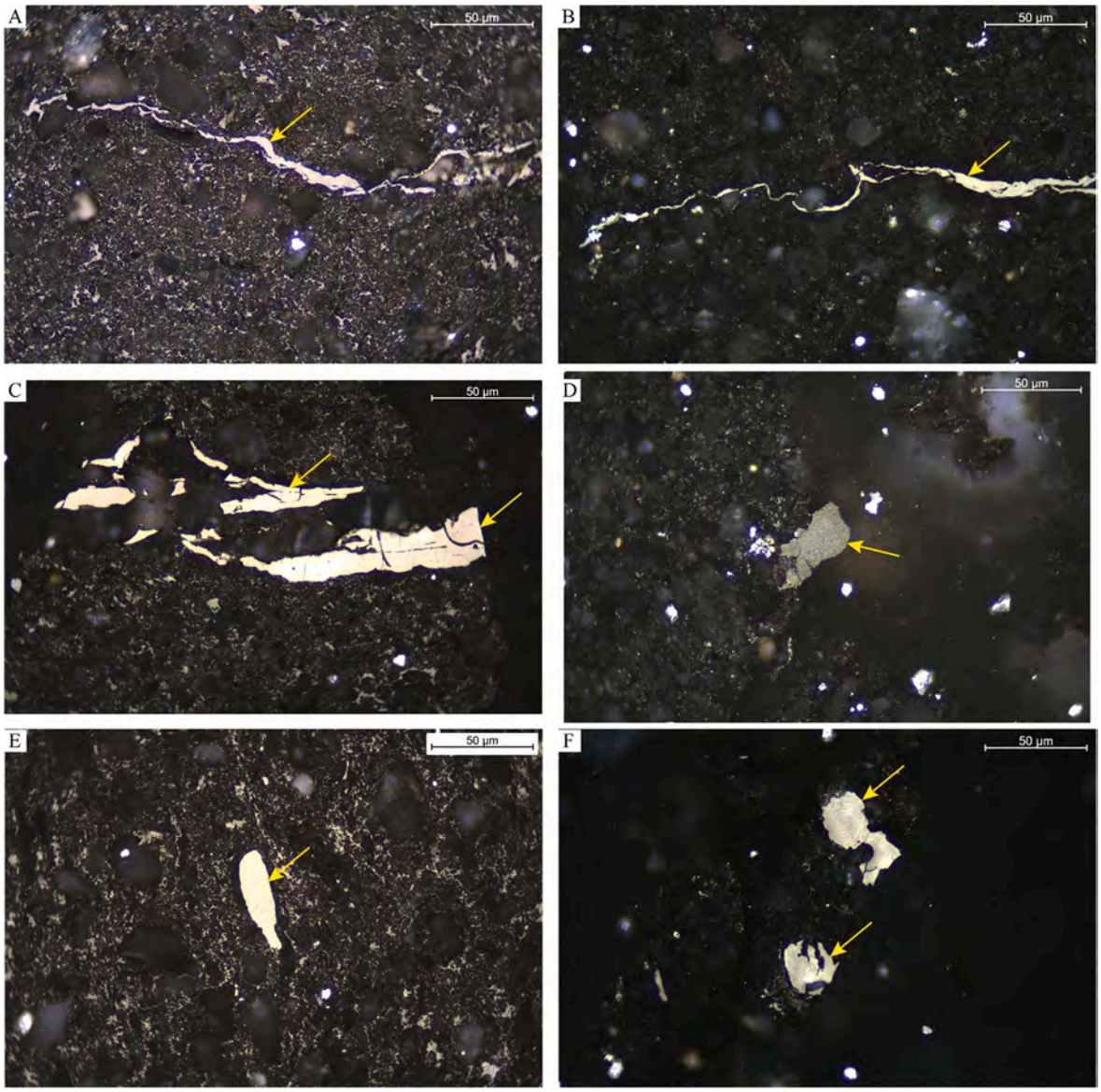

Fig. 4. Photomicrographs of graptolites in reflected white light and oil immersion. (A) Graptolite (yellow arrow), TB-28. (B) Graptolite (yellow arrow), SH-18. (C) Graptolite (yellow arrows), QL-06. (D) Granular graptolite fragments (red arrows), SH-18. (E) Graptolite fragments (yellow arrows), QL-17. The appendix at the bottom of the fragment suggests a graptolite origin. (F) Graptolite fragments (yellow arrows), SH-18. The anisotropy and concentric pattern (upper particle) suggest a graptolite origin. (For interpretation of the references to colour in this figure legend, the reader is referred to the web version of this article.)

Pyrobitumen within the clusters of clay minerals (illite) is clearly distinct from matrix bitumen filling interparticle pores between mineral grains (Fig. 3). Graptolites show typical periderm when viewed perpendicular to the bedding (Fig. 4A–C) and occur as fragments dispersed in the fine-grained matrix (Fig. 4D–F). Some graptolites in the studied samples show anisotropy under the microscope (Fig. 4F), and others (both large periderm and small fragments) appear to be granular (Fig. 4D). VLPs occur as dispersed OM particles of various shapes in the fine-grained matrix, with the shape being rounded or irregular (Fig. 5). The size of VLPs is generally >5 μm. Acritarchs occur as round OM particles with spikes on the rim (Fig. 6), with a typical size of about 10–15 μm.

4.3. Organic matter-hosted pores

OM-hosted pores are abundant in pyrobitumen, including both matrix bitumen in the fine-grained matrix (Fig. 7) and pyrobitumen mixed with clay minerals (Fig. 8). Organic pores in pyrobitumen mixed with clay minerals show weak alignment along clay flakes (Fig. 8). The size of organic pores is typically smaller than 1000 nm. The shape of organic pores is round or irregular (Figs. 7, 8).

Organic pores were not observed in non-granular graptolite, which is the main type of graptolite in the studied samples (Fig. 9). Granular graptolite, however, can host nanometer-scale organic pores (Fig. 10). Similar to graptolite, most VLPs do not have pores (Fig. 11).

5. Discussion

5.1. Thermal evolution of organic matter

Prior studies have reported the dominance of solid bitumen/pyrobitumen in over-mature shales (Hackley and Cardott, 2016; Liu et al., 2017, 2019, 2022; Mastalerz et al., 2018; Hackley et al., 2021). Thermally, the studied rocks are over mature (EqR_o 1.93%–3.07%). Oil-

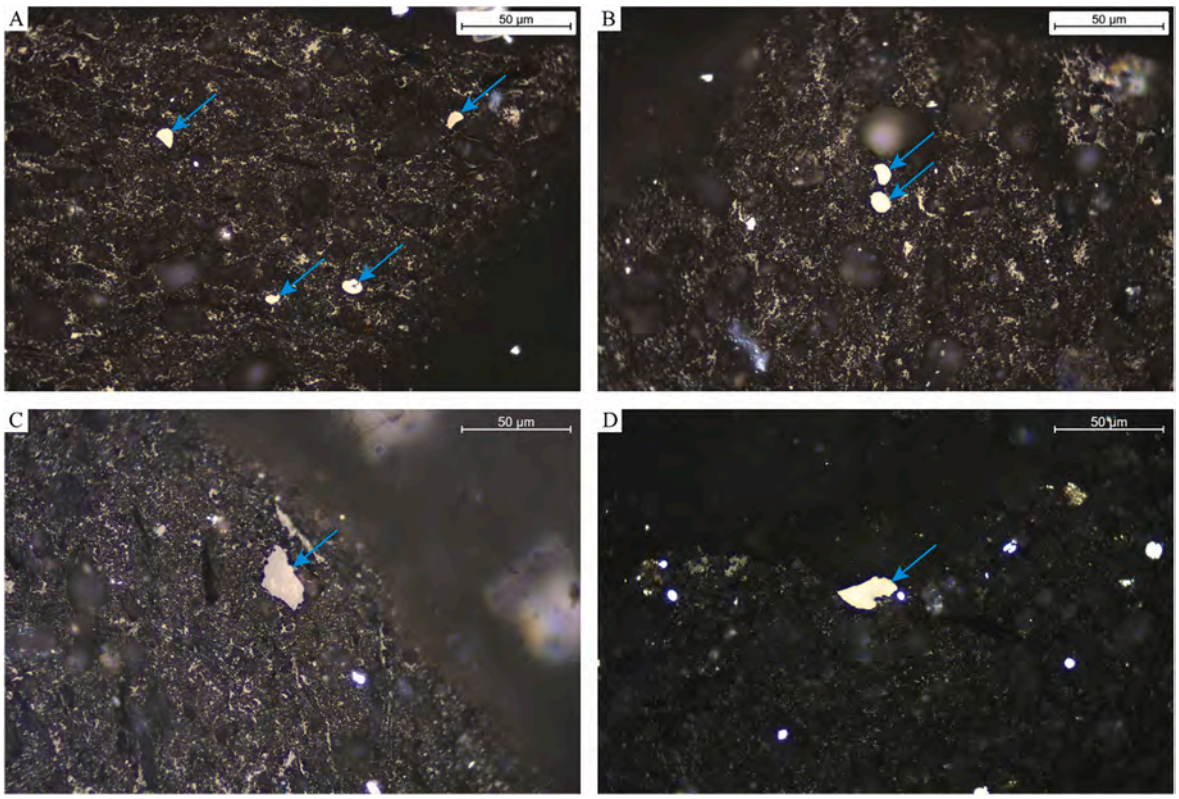

Fig. 5. Photomicrographs of vitrinite-like particles (VLP) in reflected white light and oil immersion. (A–B) Rounded to subrounded VLP (cyan arrows), QL-17. (C–D) Irregular VLP (cyan arrows), (C) TB-28, (D) SH-18. (For interpretation of the references to colour in this figure legend, the reader is referred to the web version of this article.)

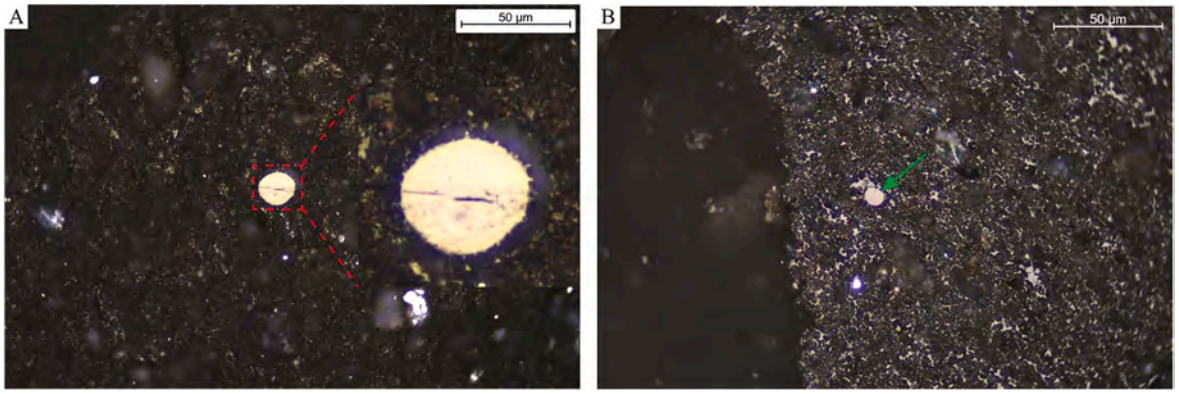

Fig. 6. Photomicrographs of acritarchs in reflected white light and oil immersion. (A) QL-17. The insert shows details of the acritarch. Note the spikes on the rim of the acritarch. (B) Acritarch (green arrow), TB-28. (For interpretation of the references to colour in this figure legend, the reader is referred to the web version of this article.)

prone macerals have finished hydrocarbon generation and now occur as pyrobitumen. Therefore, oil-prone macerals such as alginite should not exist in the studied samples. Oil-prone macerals were indeed not observed and pyrobitumen is the dominant OM in these over-mature samples (Table 2). Graptolites, VLPs, and acritarchs can still be identified on the basis of their morphology (Figs. 4–6) because of their low hydrocarbon generation potential. Wei et al. (2021) observed pyrobitumen, zooclasts, and acritarchs, and Qiu et al. (2022) identified pyrobitumen, graptolites, and VLPs in the Wufeng-Longmaxi Shale, consistent with this study. However, multiple earlier studies identified abundant algae in this over-mature black shale succession (Nie et al., 2018; Hu et al., 2020; Zhang et al., 2020a, 2020b). For example, Zhang et al. (2020b) identified acritarchs, green algae, fungi, and benthic algae in the Wufeng-Longmaxi Shale. Fungal spores and algae (Figures 4 to 6 of Zhang et al., 2020b) probably exist in the Wufeng-Longmaxi Shale, but definitely not in great abundance because they were not observed in this study. In addition, these algae and spores are definitely not oil-prone OM, because if they are, they should have transformed to hydrocarbons and pyrobitumen at this maturity and would not have been able to retain their original morphology. Hackley et al. (2017) conducted artificial thermal maturation experiments of *Tasmanites* microfossils, a type of unicellular green algae with high hydrocarbon generation potential, and found that *Tasmanites* was absent after being heated at 340 °C for 72 h ($R_o \sim 1.0\%$), consistent with the absence of *Tasmanites* cysts in naturally matured samples (Ryder et al., 2013). Luo et al. (2021) also found that algae-derived OM such as alginite and bituminite in the immature

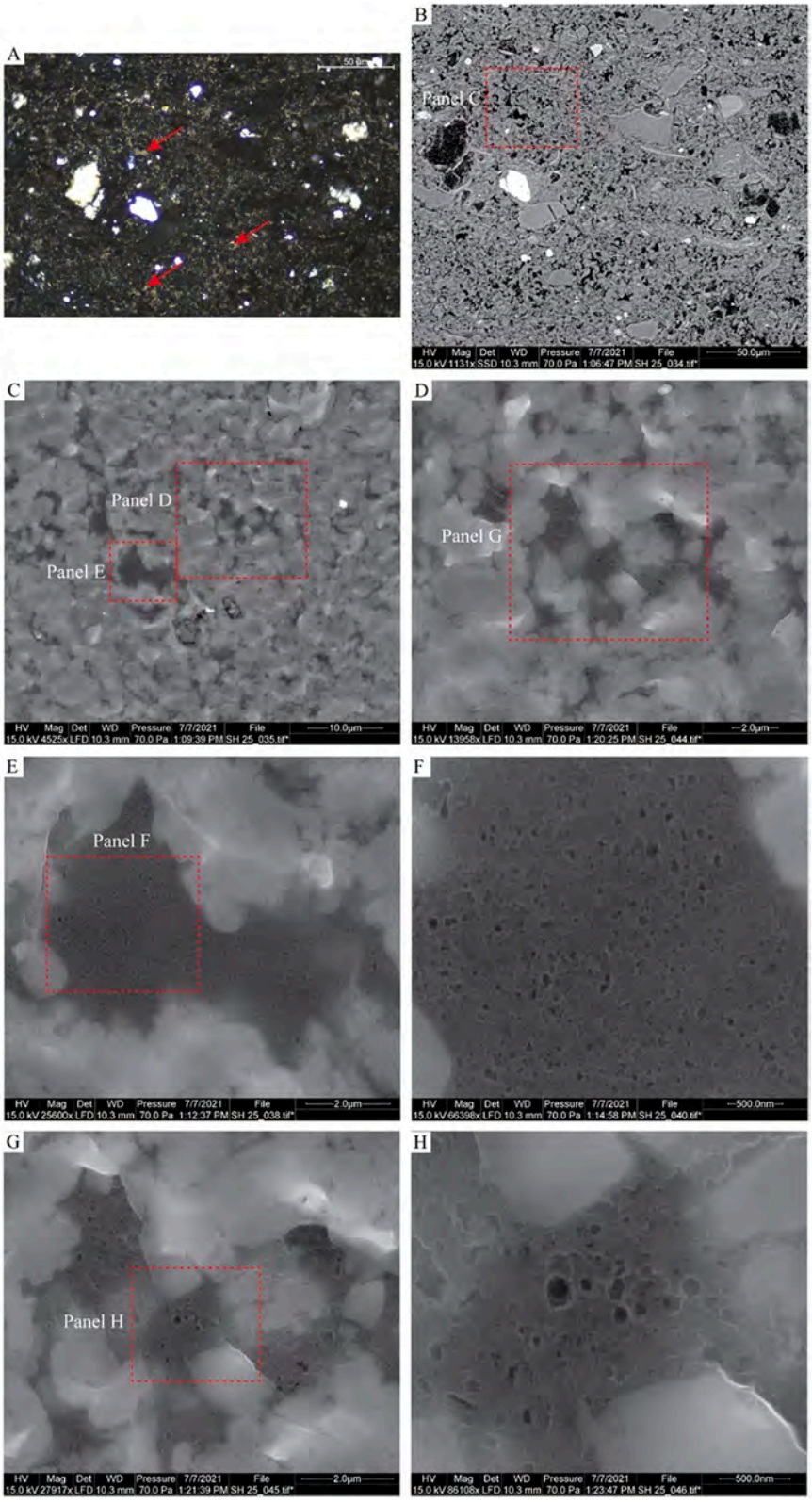

Fig. 7. Photomicrographs of pyrobitumen in the fine-grained matrix. (A) Pyrobitumen (red arrows) in reflected white light and oil immersion. (B) The same field of view as panel A under the SEM (backscattered electron mode). (C–H) Details of pyrobitumen with organic pores under the SEM (secondary electron mode). Panels F and H are the close-up views of the red dashed areas in panels E and G, respectively. Sample SH-25. (For interpretation of the references to colour in this figure legend, the reader is referred to the web version of this article.)

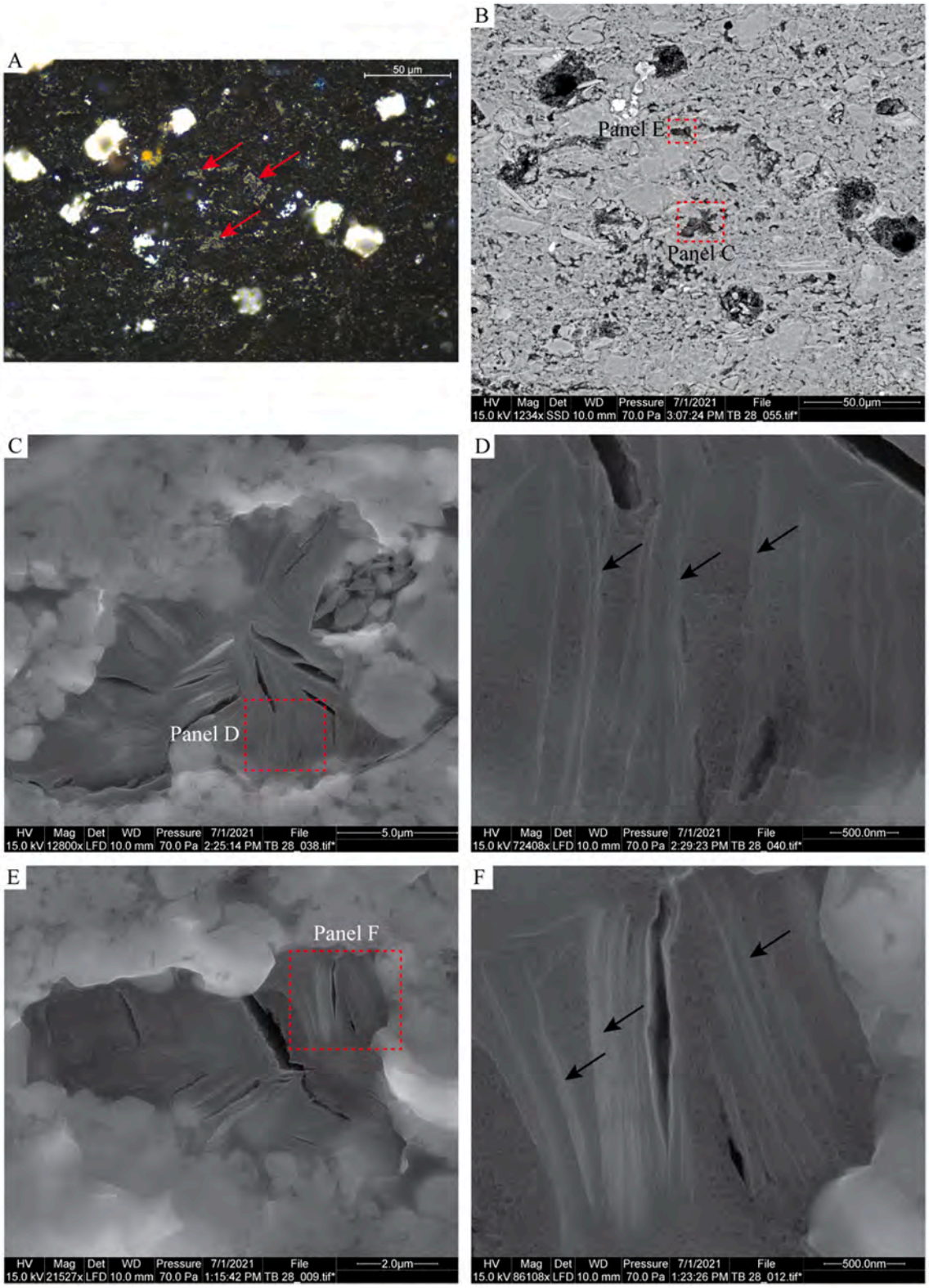

Fig. 8. Photomicrographs of pyrobitumen mixed with clay minerals. (A) Pyrobitumen (red arrows) in reflected white light and oil immersion. (B) The same field of view as panel A under the SEM (backscattered electron mode). (C – F) Details of pyrobitumen with organic pores under the SEM (secondary electron mode). Panels D and F are the close-up views of the red dashed areas in panels C and E, respectively. Pyrobitumen is mixed with illite (black arrows). Illite is clearly diagenetic clay mineral that grew in bitumen. Sample TB-28. (For interpretation of the references to colour in this figure legend, the reader is referred to the web version of this article.)

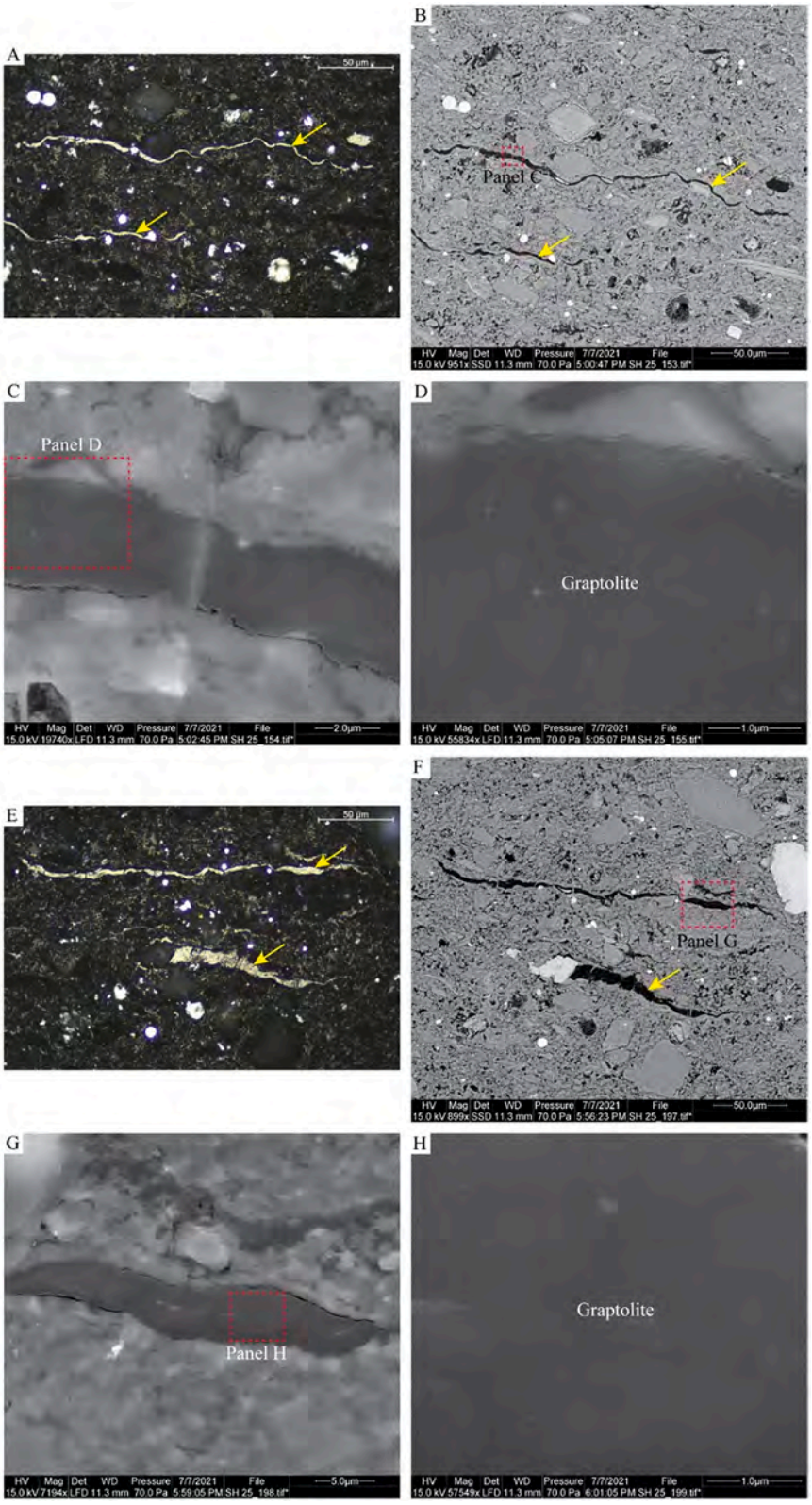

Fig. 9. Photomicrographs of graptolites without organic pores. (A, E) Graptolite (yellow arrows) in reflected white light and oil immersion. (B, F) The same fields of view as panels A and E under the SEM (backscattered electron mode), respectively. (C–D, G–H,) Details of graptolites under the SEM (secondary electron mode). Panels D and H are the close-up views of the red dashed areas in panels C and G, respectively. No pores were observed in graptolites. Sample SH-25. (For interpretation of the references to colour in this figure legend, the reader is referred to the web version of this article.)

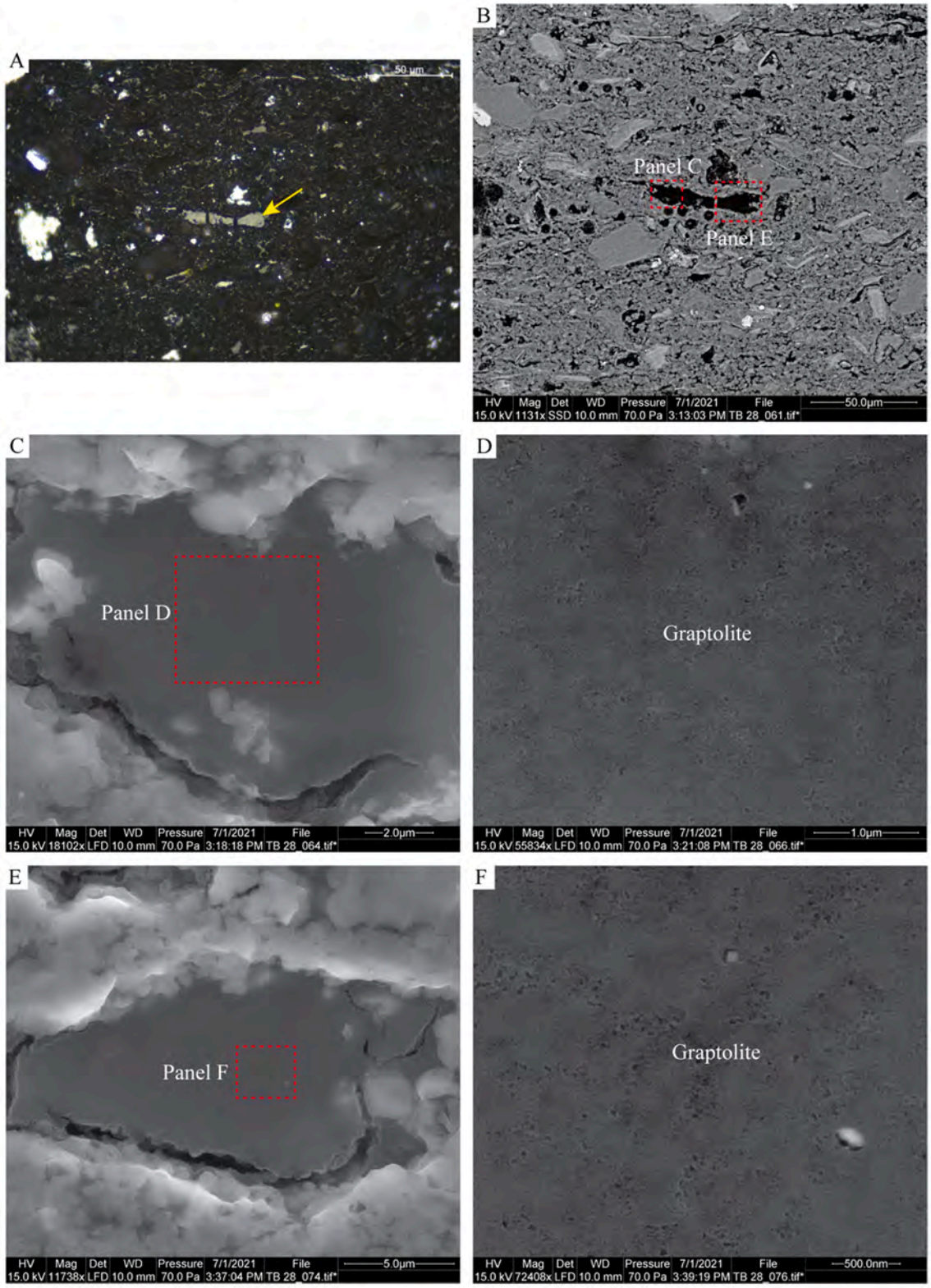

Fig. 10. Photomicrographs of granular graptolites with organic pores. (A) Granular graptolite (yellow arrow) in reflected white light and oil immersion. (B) The same field of view as panel A under the SEM (backscattered electron mode). (C – F) Details of graptolites under the SEM (secondary electron mode). Panels D and F are the close-up views of the red dashed areas in panels C and E, respectively. Nanometer-scale pores occur in granular graptolites. Sample TB-28. (For interpretation of the references to colour in this figure legend, the reader is referred to the web version of this article.)

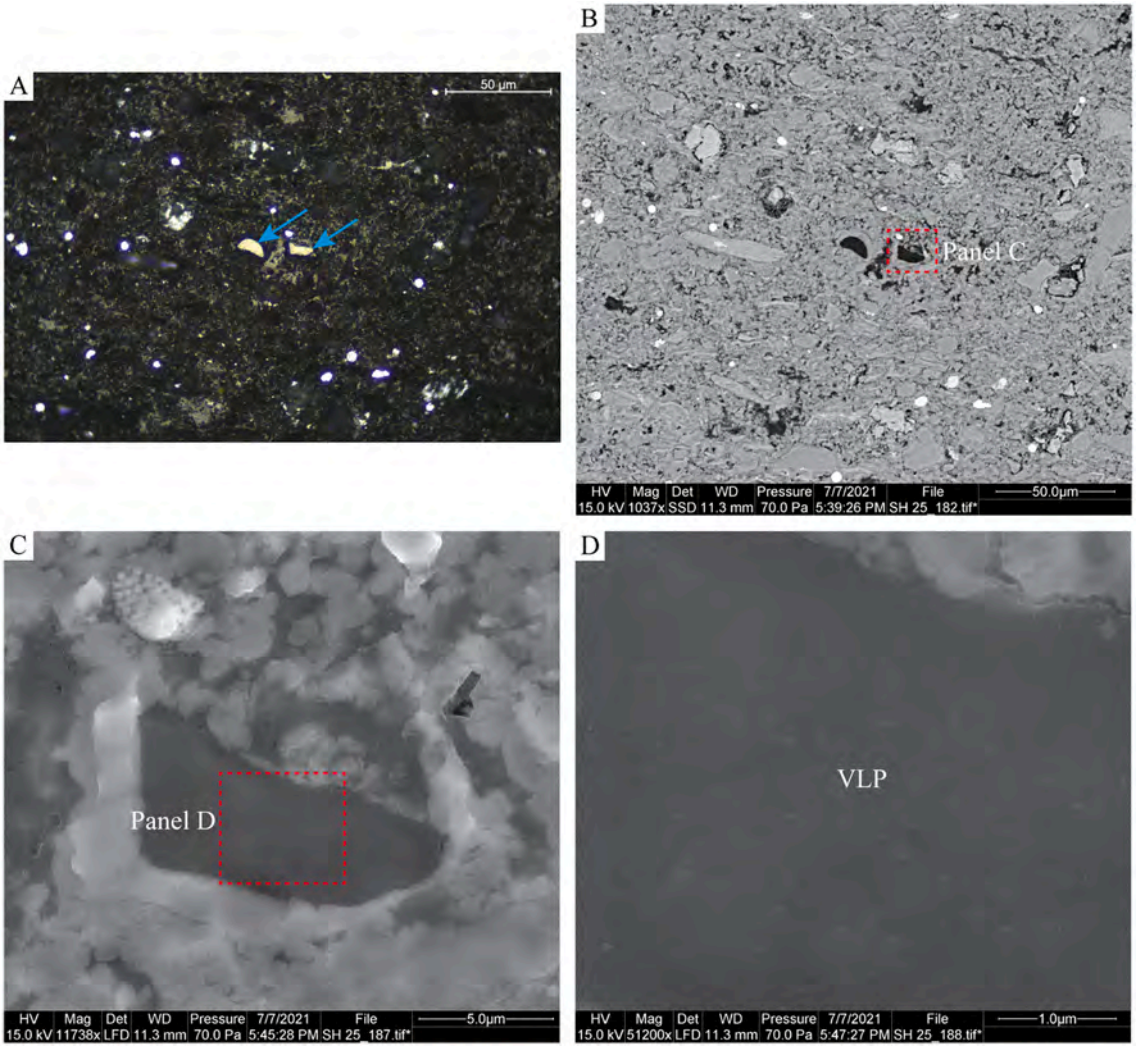

Fig. 11. Photomicrographs of vitrinite-like particles (VLPs). (A) VLPs (cyan arrows) in reflected white light and oil immersion. (B) The same field of view as panel A under the SEM (backscattered electron mode). (C – D) Details of VLPs under the SEM (secondary electron mode). Panel D is the close-up view of the red dashed areas in panel C. No pores were observed in VLPs. Sample SH-25. (For interpretation of the references to colour in this figure legend, the reader is referred to the web version of this article.)

Proterozoic Xiamaling shales from China and the Cambrian Alum shales from Sweden decomposed after being heated from 325 °C to 350 °C for 72 (R_o 1.11–1.48%) and solid bitumen dominates OM composition afterwards, supporting the absence of oil-prone alginite in the over-mature Wufeng-Longmaxi Shale. Artificial thermal maturation experiments of graptolite-bearing sediments show that graptolite reflectance and vitrinite reflectance increase with heating temperature at a similar rate, and that graptolite random reflectance is a good indicator of thermal maturity (Luo et al., 2018; Wang et al., 2020).

5.2. Maceral control on organic pore development

OM type critically controls the development of organic pores in black shales (Liu et al., 2017, 2022; Katz and Arango, 2018; Ardakani et al., 2018; Wu et al., 2020; Wei et al., 2021; Delle Piane et al., 2022). Oil-prone macerals generate oil and gas and transform to solid bitumen during thermal maturation, and subsequently organic pores develop in solid bitumen (Cardott et al., 2015; Liu et al., 2017, 2022; Mastalerz et al., 2018). Cardott et al. (2015) observed a solid bitumen network with nano-scale pores in the Woodford Shale. In comparison, gas-prone and inert macerals rarely develop organic pores due to their low hydrocarbon generation potential (Ardakani et al., 2018; Mastalerz et al., 2018; Liu et al., 2022). In this study, organic pores mainly occur in

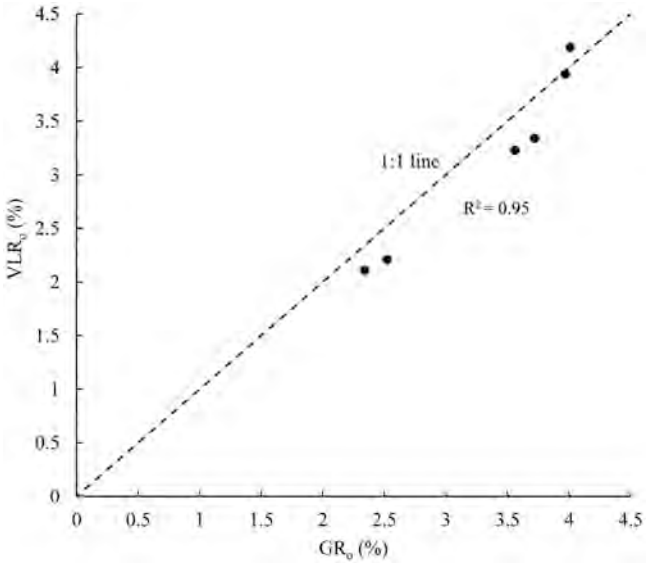

Fig. 12. Graph showing relationship between graptolite reflectance (GR_o) and vitrinite-like particle reflectance (VLR_o). Although most data points are not exactly on the 1:1 line, they are distributed near the 1:1 line.

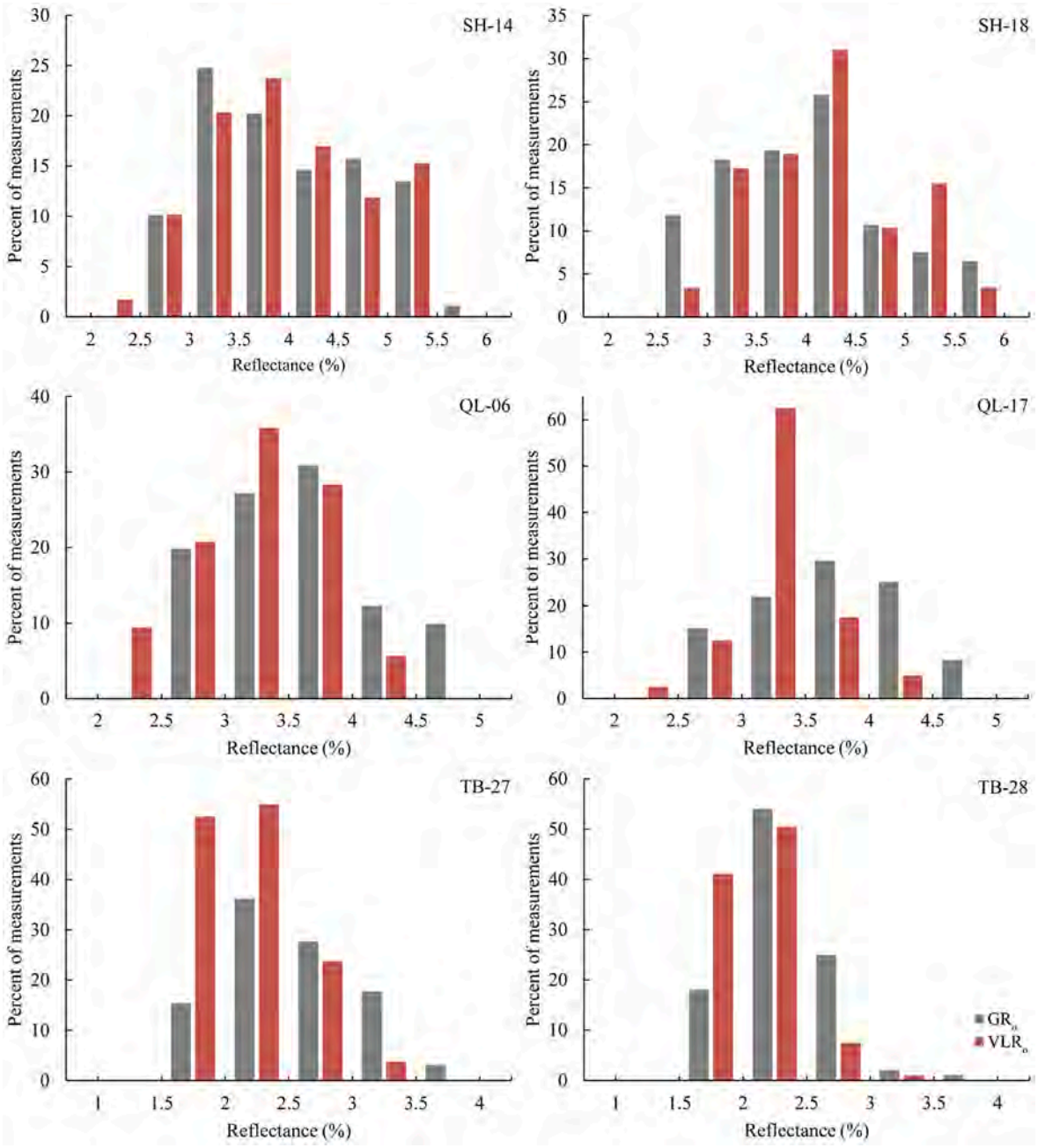

Fig. 13. Histograms of measured graptolite reflectance (GR_o) and virinite-like particle reflectance (VLR_o).

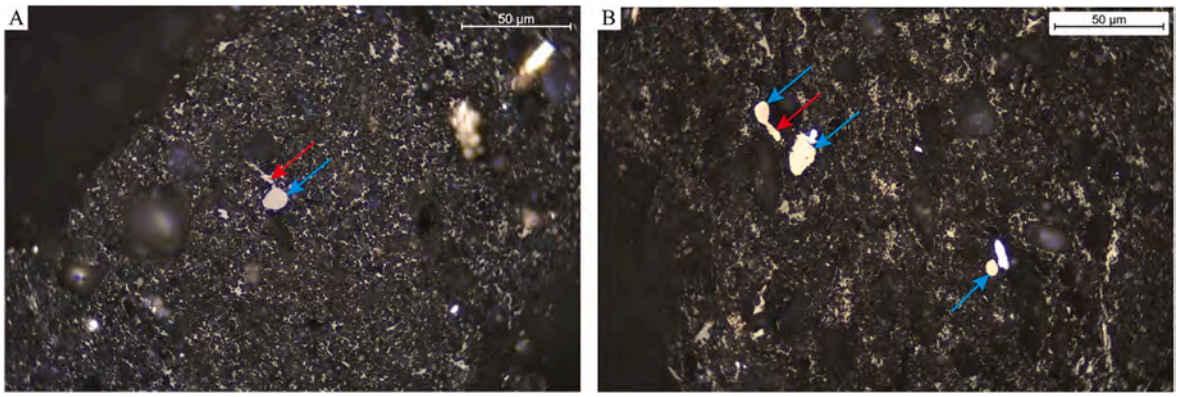

Fig. 14. Photomicrographs of irregular vitrinite-like particles (VLPs) (cyan arrows) in reflected white light and oil immersion. The appendices (red arrows) suggest that these VLPs are fragments of the organic remains of organisms, most likely graptolites. (A) TB-28, (B) QL-17. (For interpretation of the references to colour in this figure legend, the reader is referred to the web version of this article.)

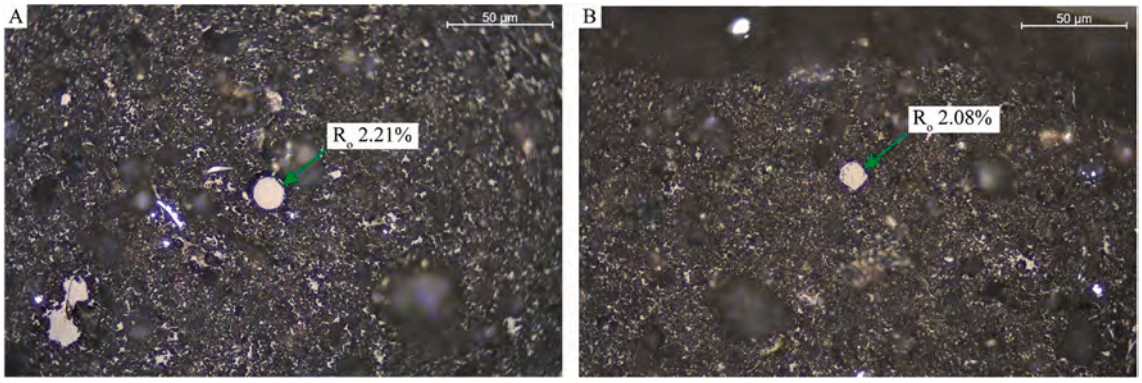

Fig. 15. Photomicrographs of acritarchs (A) and round vitrinite-like particles (VLPs) (B) in reflected white light and oil immersion. The VLP in B has similar reflectance and morphology to the acritarch in A, suggesting that the VLP is probably derived from acritarchs. TB-28.

pyrobitumen (Figs. 7, 8), and minor nano-scale pores are present in granular graptolites (Fig. 10). Yang et al. (2020) and Delle Piane et al. (2022) also found that SEM-visible organic pores are pervasive in pyrobitumen and undeveloped in graptolites in the Wufeng-Longmaxi Shale. Similarly, Wei et al. (2021) reported that organic pores in the Wufeng-Longmaxi Shale are primarily hosted by pyrobitumen, and that zooclasts contribute little to porosity. However, multiple studies have described organic pores within graptolites in the Wufeng-Longmaxi Shale (e.g., Luo et al., 2016; Ma et al., 2016; Qiu et al., 2018; Gong et al., 2020; Tenger et al., 2021). Whether these organic pores in graptolites are primary or secondary remains unclear at present (Liu et al., 2022). Organic pores in over-mature shales are primarily hosted by pyrobitumen. Because pyrobitumen was once liquid, it may form an interconnected network of pyrobitumen with organic pores, forming an organic pore network in shale reservoirs (Liu et al., 2019; Delle Piane et al., 2022).

5.3. Origin of vitrinite-like particles

Vitrinite-like particles are OM particles that resemble vitrinite (Buchardt and Lewan, 1990). The reflectance of VLPs can be used to estimate the thermal maturity of host rocks when vitrinite is absent, especially in pre-Devonian rocks (Buchardt and Lewan, 1990; Xiao et al., 2000; Petersen et al., 2013; Teng et al., 2020; Luo et al., 2020). VLPs are widely present in shale formations and their origin is still a matter of debate (Luo et al., 2021). Some studies suggest that VLPs are solid bitumen that is indistinguishable from vitrinite (Hackley and Lewan, 2018; Schmidt et al., 2019), whereas others argue that VLP are syndepositional OM (Petersen et al., 2013; Liu et al., 2020; Luo et al., 2021). Luo et al. (2021), based on the fluorescence variation from bituminite to VLP, similar morphology and texture between bituminite and VLP, and their co-evolution behavior during artificial thermal maturation experiments, concluded that VLP in the Proterozoic Xiamaling shales is a biodegradation product of bituminite. On the other hand, they suggested that VLP in the Cambrian Alum shales is derived from akinete cells on the basis of their spherical or oval shape, rigidity, and occurrence.

In this study, VLPs (average 6.8 vol%) are minor constituents of OM in the studied shales (Figs. 5, 11). We speculate that VLPs in the Wufeng-Longmaxi Shale are of syndepositional origin, with irregular ones being derived from graptolite fragments and round ones from acritarchs. The former assumption is supported by abundance of graptolites in this black shale succession (Table 2; Luo et al., 2016, 2017, 2018; Wang et al., 2019, 2020, 2021), the observation that the average reflectance of VLPs is close to that of graptolites (Fig. 12), and that the histograms of VLR$_o$ are similar to those of GR$_o$ (Fig. 13). In addition, some VLPs have what appear to be appendices, suggestive of a graptolite origin (Fig. 14). Petersen et al. (2013), based on the identical reflectance distribution of graptolites and VLPs, suggested that VLPs in Lower Paleozoic shales in southern Scandinavia are fragments of graptolites that have lost recognizable morphology. The round VLPs are probably derived from acritarchs as they have similar morphology and reflectance values (Fig. 15). The reflectance of VLPs cannot be compared with that of acritarchs statistically because acritarchs are rare (average 0.3 vol%) in the studied samples. Solid bitumen has been reported to fill fossil cavities, such as foramnifera tests, and OM infills generally show organic pores (Loucks and Reed, 2014; Milliken et al., 2014; Schieber et al., 2016). In this study, VLPs in siliceous shells are generally not porous (Fig. 11) and do not contain mineral inclusions as observed in pyrobitumen (Fig. 8), suggesting syndepositional origin.

6. Conclusions

Detailed organic petrographic and SEM observations of OM in the Wufeng-Longmaxi Shale, Sichuan Basin revealed the origin of OM and the control of maceral type on the development of OM-hosted pores in this over-mature black shale succession. OM in the Wufeng-Longmaxi Shale consists of pyrobitumen, graptolites, VLPs, and acritarchs, with pyrobitumen and graptolites being the dominant OM (> 90 vol% of total OM based on point counting). Oil-prone alginite does not exist in the Wufeng-Longmaxi Shale due to hydrocarbon generation. Pyrobitumen occurs as matrix bitumen in the fine-grained matrix as well as within clusters of diagenetic clay minerals and in fossil cavities. Maceral composition has an important control on the development of OM-hosted pores. Organic pores are primarily hosted by pyrobitumen and are rare in other macerals. VLPs are minor in the Wufeng-Longmaxi Shale and are of syndepositional origin. They are likely derived from graptolite fragments without diagnostic features or acritarchs, as suggested by similar average reflectance, reflectance distribution, and morphology.

Declaration of Competing Interest

The authors declare that they have no known competing financial interests or personal relationships that could have appeared to influence the work reported in this paper.

Acknowledgements

This research was supported by the National Science Foundation of China (Grant No. 42102194) and the sponsors of the Indiana University Shale Research Consortium (Anadarko, Chevron, ConocoPhillips, ExxonMobil, Shell, Statoil, Marathon, Whiting, Wintershall). An NSF equipment grant to Juergen Schieber (EAR-0318769) provided funds for the purchase of the analytical SEM that was used for acquiring the SEM images used in this study. Bei Liu was also partially supported by the U. S. Department of Energy, Office of Science, Office of Basic Energy Sciences, Chemical Sciences, Geosciences, and Biosciences Division under

Award No. DE-SC0006978. Many thanks to Dr. Zhen Qiu from PetroChina Research Institute of Petroleum Exploration & Development for help with collecting samples in the field.

References

Ardakani, O.H., Sanei, H., Ghanizadeh, A., Lavoie, D., Chen, Z., Clarkson, C.R., 2018. Do all fractions of organic matter contribute equally in shale porosity? A case study from Upper Ordovician Utica Shale, southern Quebec, Canada. Mar. Pet. Geol. 92, 794–808.

ASTM, 2015. D2797 Standard Practice for Preparing Coal Samples for Microscopical Analysis by Reflected Light. ASTM International, West Conshohocken, PA.

Buchardt, B., Lewan, M.D., 1990. Reflectance of vitrinite-like macerals as a thermal maturity index for Cambrian–Ordovician Alum Shale, southern Scandinavia. AAPG Bull. 74, 394–406.

Cardott, B.J., Curtis, M.E., 2018. Identification and nanoporosity of macerals in coal by scanning electron microscopy. Int. J. Coal Geol. 190, 205–217.

Cardott, B.J., Landis, C.R., Curtis, M.E., 2015. Post-oil solid bitumen network in the Woodford Shale, USA—a potential primary migration pathway. Int. J. Coal Geol. 139, 106–113.

Chen, S., Zhang, C., Li, X., Zhang, Y., Wang, X., 2021. Simulation of methane adsorption in diverse organic pores in shale reservoirs with multi-period geological evolution. International Journal of Coal Science & Technology 8, 844–855.

Delle Piane, C., Ansari, H., Li, Z., Mata, J., Rickard, W., Pini, R., Dewhurst, D.N., Sherwood, N., 2022. Influence of organic matter type on porosity development in the Wufeng-Longmaxi Shale: a combined microscopy, neutron scattering and physisorption approach. Int. J. Coal Geol. 249, 103880.

Flores, D., Suárez-Ruiz, I., 2017. Organic petrology in the study of dispersed organic matter. In: Suárez-Ruiz, I., Filho, J.G.M. (Eds.), The Role of Organic Petrology in the Exploration of Conventional and Unconventional Hydrocarbon Systems. Bentham Science Publishers, Sharjah, pp. 34–76.

Gong, J., Qiu, Z., Zou, C., Wang, H., Shi, Z., 2020. An integrated assessment system for shale gas resources associated with graptolites and its application. Appl. Energy 262, 114524.

Hackley, P.C., Cardott, B.J., 2016. Application of organic petrography in North American shale petroleum systems: a review. Int. J. Coal Geol. 163, 8–51.

Hackley, P.C., Lewan, M., 2018. Understanding and distinguishing reflectance measurements of solid bitumen and vitrinite using hydrous pyrolysis: implications to petroleum assessment. AAPG Bull. 102, 1119–1140.

Hackley, P.C., Walters, C.C., Kelemen, S.R., Mastalerz, M., Lowers, H.A., 2017. Organic petrology and micro-spectroscopy of Tasmanites microfossils: applications to kerogen transformations in the early oil window. Org. Geochem. 114, 23–44.

Hackley, P.C., Jubb, A.M., McAleer, R.J., Valentine, B.J., Birdwell, J.E., 2021. A review of spatially resolved techniques and applications of organic petrography in shale petroleum systems. Int. J. Coal Geol. 241, 103745.

Hao, F., Zou, H., Lu, Y., 2013. Mechanisms of shale gas storage: implications for shale gas exploration in China. AAPG Bull. 97, 1325–1346.

Hu, G., Pang, Q., Jiao, K., Hu, C., Liao, Z., 2020. Development of organic pores in the Longmaxi Formation overmature shales: combined effects of thermal maturity and organic matter composition. Mar. Pet. Geol. 116, 104314.

Katz, B.J., Arango, I., 2018. Organic porosity: a geochemist's view of the current state of understanding. Org. Geochem. 123, 1–16.

Li, Y., Schieber, J., Fan, T., Li, Z., Zhang, J., 2017. Regional depositional changes and their controls on carbon and sulfur cycling across the Ordovician-Silurian boundary, northwestern Guizhou, South China. Palaeogeogr. Palaeoclimatol. Palaeoecol. 485, 816–832.

Liu, B., Schieber, J., Mastalerz, M., 2017. Combined SEM and reflected light petrography of organic matter in the New Albany Shale (Devonian-Mississippian) in the Illinois Basin: a perspective on organic pore development with thermal maturation. Int. J. Coal Geol. 184, 57–72.

Liu, B., Schieber, J., Mastalerz, M., 2019. Petrographic and micro-FTIR study of organic matter in the Upper Devonian New Albany Shale during thermal maturation: implications for kerogen transformation. In: Camp, W., Milliken, K., Taylor, K., Fishman, N., Hackley, P., Macquaker, J. (Eds.), Mudstone Diagenesis: Research Perspectives for Shale Hydrocarbon Reservoirs, Seals, and Source Rocks, AAPG Memoir, vol. 120, pp. 165–188.

Liu, B., Teng, J., Mastalerz, M., Schieber, J., 2020. Assessing the thermal maturity of black shales using vitrinite reflectance: insights from Devonian black shales in the eastern United States. Int. J. Coal Geol. 220, 103426.

Liu, B., Teng, J., Mastalerz, M., Schieber, J., Schimmelmann, A., Bish, D., 2021. Compositional control on shale pore structure characteristics across a maturation gradient: insights from the Devonian New Albany Shale and Marcellus Shale in the eastern United States. Energy Fuel 35, 7913–7929.

Liu, B., Mastalerz, M., Schieber, J., 2022. SEM petrography of dispersed organic matter in black shales: a review. Earth Sci. Rev. 224, 103874.

Loucks, R.G., Reed, R.M., 2014. Scanning-electron-microscope petrographic evidence for distinguishing organic-matter pores associated with depositional organic matter versus migrated organic matter in mudrocks. Gulf Coast Assoc. Geol. Soc. J. 3, 51–60.

Loucks, R.G., Reed, R.M., Ruppel, S.C., Jarvie, D.M., 2009. Morphology, genesis, and distribution of nanometer-scale pores in siliceous mudstones of the Mississippian Barnett Shale. J. Sediment. Res. 79, 848–861.

Loucks, R.G., Reed, R.M., Ruppel, S.C., Hammes, U., 2012. Spectrum of pore types and networks in mudrocks and a descriptive classification for matrix-related mudrock pores. AAPG Bull. 96, 1071–1098.

Luo, Q., Zhong, N., Dai, N., Zhang, W., 2016. Graptolite-derived organic matter in the Wufeng–Longmaxi Formations (Upper Ordovician–Lower Silurian) of southeastern Chongqing, China: implications for gas shale evaluation. Int. J. Coal Geol. 153, 87–98.

Luo, Q., Hao, J., Skovsted, C.B., Luo, P., Khan, I., Wu, J., Zhong, N., 2017. The organic petrology of graptolites and maturity assessment of the Wufeng–Longmaxi Formations from Chongqing, China: insights from reflectance cross-plot analysis. Int. J. Coal Geol. 183, 161–173.

Luo, Q., Hao, J., Skovsted, C.B., Xu, Y., Liu, Y., Wu, J., Zhang, S., Wang, W., 2018. Optical characteristics of graptolite-bearing sediments and its implication for thermal maturity assessment. Int. J. Coal Geol. 195, 386–401.

Luo, Q., Fariborz, G., Zhong, N., Wang, Y., Qiu, N., Skovsted, C.B., Suchý, V., Schovsbo, N.H., Morga, R., Xu, Y., Hao, J., Liu, A., Wu, J., Cao, W., Min, X., Wu, J., 2020. Graptolites as fossil geo-thermometers and source material of hydrocarbons: an overview of four decades of progress. Earth Sci. Rev. 200, 103000.

Luo, Q., Zhang, L., Zhong, N., Wu, J., Goodarzi, F., Sanei, H., Skovsted, C.B., Suchý, V., Li, M., Ye, X., Cao, W., Liu, A., Min, X., Pan, Y., Yao, L., Wu, J., 2021. Thermal evolution behavior of the organic matter and a ray of light on the origin of vitrinite-like maceral in the Mesoproterozoic and lower Cambrian black shales: insights from artificial maturation. Int. J. Coal Geol. 244, 103813.

Ma, Y., Zhong, N., Cheng, L., Pan, Z., Dai, N., Zhang, Y., Yang, L., 2016. Pore structure of the graptolite-derived OM in the Longmaxi Shale, southeastern Upper Yangtze Region, China. Mar. Pet. Geol. 72, 1–11.

Mastalerz, M., Schieber, J., 2017. Effect of ion milling on the perceived maturity of shale samples: implications for organic petrography and SEM analysis. Int. J. Coal Geol. 183, 110–119.

Mastalerz, M., Drobniak, A., Stankiewicz, A.B., 2018. Origin, properties, and implications of solid bitumen in source-rock reservoirs: a review. Int. J. Coal Geol. 195, 14–36.

Milliken, K.L., Ko, L.T., Pommer, M., Marsaglia, K.M., 2014. SEM petrography of Eastern Mediterranean sapropels: analogue data for assessing organic matter in oil and gas shales. J. Sediment. Res. 84, 961–974.

Nie, H., Jin, Z., Zhang, J., 2018. Characteristics of three organic matter pore types in the Wufeng-Longmaxi Shale of the Sichuan Basin, Southwest China. Sci. Rep. 8, 1–11.

Nie, H., Chen, Q., Zhang, G., Sun, C., Wang, P., Lu, Z., 2021. An overview of the characteristic of typical Wufeng–Longmaxi shale gas fields in the Sichuan Basin, China. Nat. Gas Ind. B 8, 217–230.

Petersen, H.I., Schovsbo, N.H., Nielsen, A.T., 2013. Reflectance measurements of zooclasts and solid bitumen in Lower Paleozoic shales, southern Scandinavia: correlation to vitrinite reflectance. Int. J. Coal Geol. 114, 1–18.

Potter, J., Stasiuk, L.D., Cameron, A.R., 1998. A Petrographic Atlas of Canadian Coal Macerals and Dispersed Organic Matter. Canadian Society for Coal Science and Organic Petrology–Geological Survey of Canada (Calgary)-Canmet Energy Technology Centre (105 pp.).

Qiu, Z., Zou, C., 2020. Controlling factors on the formation and distribution of "sweet-spot areas" of marine gas shales in South China and a preliminary discussion on unconventional petroleum sedimentology. J. Asian Earth Sci. 194, 103989.

Qiu, L., Yan, D.P., Tang, S.L., Wang, Q., Yang, W.X., Tang, X., Wang, J., 2016. Mesozoic geology of southwestern China: Indosinian foreland overthrusting and subsequent deformation. J. Asian Earth Sci. 122, 91–105.

Qiu, Z., Zou, C., Li, X., Wang, H., Dong, D., Lu, B., Zhou, S., Shi, Z., Feng, Z., Zhang, M., 2018. Discussion on the contribution of graptolite to organic enrichment and gas shale reservoir: a case study of the Wufeng–Longmaxi shales in South China. J. Nat. Gas Geosci. 3, 147–156.

Qiu, Z., Zou, C., Wang, H., Dong, D., Lu, B., Chen, Z., Liu, D., Li, G., Liu, H., He, J., Wei, L., 2020. Discussion on the characteristics and controlling factors of differential enrichment of shale gas in the Wufeng-Longmaxi formations in south China. J. Nat. Gas Geosci. 5, 117–128.

Qiu, Z., Liu, B., Lu, B., Shi, Z., Li, Z., 2022. Mineralogical and petrographic characteristics of the Ordovician-Silurian Wufeng-Longmaxi Shale in the Sichuan Basin and implications for depositional conditions and diagenesis of black shales. Mar. Pet. Geol. 135, 105428.

Ross, D.J.K., Bustin, R.M., 2009. The importance of shale composition and pore structure upon gas storage potential of shale gas reservoirs. Mar. Pet. Geol. 26, 916–927.

Schieber, J., 1996. Early diagenetic silica deposition in algal cysts and spores: a source of sand in black shales? J. Sediment. Res. 66, 175–183.

Schieber, J., 2010. Common themes in the formation and preservation of intrinsic porosity in shales and mudstones-illustrated with examples across the Phanerozoic. In: SPE Unconventional Gas Conference. Society of Petroleum Engineers, Pittsburgh, Pennsylvania, USA (February 23–25, 2010, SPE Paper 132370, 10 pp.).

Schieber, J., 2013. SEM observations on ion-milled samples of Devonian black shales from Indiana and New York: the petrographic context of multiple pore types. In: Camp, W., Diaz, E., Wawak, B. (Eds.), Electron Microscopy of Shale Hydrocarbon Reservoirs. AAPG Memoir 102, pp. 153–171.

Schieber, J., Lazar, R., Bohacs, K., Klimentidis, R., Dumitrescu, M., Ottmann, J., 2016. An SEM study of porosity in the Eagle Ford Shale of Texas—Pore types and porosity distribution in a depositional and sequence-stratigraphic Context. In: Breyer, J.A. (Ed.), The Eagle Ford Shale: A Renaissance in U.S. Oil Production. AAPG Memoir 110, pp. 167–186.

Schmidt, J.S., Menezes, T.R., Souza, I.V.A.F., Spigolon, A.L.D., Pestilho, A.L.S., Coutinho, L.F.C., 2019. Comments on empirical conversion of solid bitumen reflectance for thermal maturity evaluation. Int. J. Coal Geol. 201, 44–50.

Schoenherr, J., Littke, R., Urai, J.L., Kukla, P.A., Rawahi, Z., 2007. Polyphase thermal evolution in the Infra-Cambrian Ara Group (South Oman Salt Basin) as deduced by maturity of solid reservoir bitumen. Org. Geochem. 38, 1293–1318.
Stasiuk, L.D., Burgess, J., Thompson-Rizer, C., Hutton, A., Cardott, B., 2002. Status report on TSOP-ICCP dispersed organic matter classification working group. Soc. Organ. Petrol. Newslett. 19 (3), 14.
Suárez-Ruiz, I., Flores, D., Mendonça Filho, J.G., Hackley, P.C., 2012. Review and update of the applications of organic petrology: part 1, geological applications. Int. J. Coal Geol. 99, 54–112.
Sun, C., Nie, H., Dang, W., Chen, Q., Zhang, G., Li, W., Lu, Z., 2021. Shale gas exploration and development in China: current status, geological challenges, and future directions. Energy Fuel 35, 6359–6379.
Teichmüller, M., Ottenjann, K., 1977. Art und Diagenese von Liptiniten und lipoiden Stoffen in einem Erdölmuttergestein aufgrund fluoroeszenzmikroskopischer Untersuchungen. Erdöl Kohle Erdgas 30 (9), 387–398.
Teng, J., Mastalerz, M., Liu, B., Gognat, T., Hauser, E., McLaughlin, P., 2020. Variations of organic matter transformation in response to hydrothermal fluids: example from the Indiana part of the Illinois Basin. Int. J. Coal Geol. 219, 103410.
Teng, J., Mastalerz, M., Liu, B., 2021. Petrographic and chemical structure characteristics of amorphous organic matter in marine black shales: insights from Pennsylvanian and Devonian black shales in the Illinois Basin. Int. J. Coal Geol. 235, 103676.
Tenger, B., Lu, L., Yu, L., Zhang, W., Pan, A., Shen, B., Wang, Y., Yang, Y., Gao, Z., 2021. Formation, preservation and connectivity control of organic pores in shale. Pet. Explor. Dev. 48, 687–699.
Tissot, B.P., Welte, D.H., 1984. Petroleum Formation and Occurrence, 2nd ed. Springer-Verlag, Berlin. (699 pp.).
Wang, Y., Qiu, N., Borjigin, T., Shen, B., Xie, X., Ma, Z., Lu, C., Yang, Y., Yang, L., Cheng, L., Fang, G., Cui, Y., 2019. Integrated assessment of thermal maturity of the Upper Ordovician–lower Silurian Wufeng–Longmaxi shale in Sichuan Basin, China. Mar. Pet. Geol. 100, 447–465.
Wang, Y., Qiu, N., Ma, Z., Ning, C., Zheng, L., Zhou, Y., Fang, G., Rui, X., Rao, D., 2020. Evaluation of equivalent relationship between vitrinite reflectance and solid bitumen reflectance. J. China Univ. Min. Technol. 49 (3), 563–575.
Wang, Y., Qiu, N., Xie, X., Ma, Z., Li, L., Feng, Q., Yang, L., Shen, B., Borjigin, T., Tao, N., 2021. Maturity and thermal evolution differences between two sets of Lower Palaeozoic shales and its significance for shale gas formation in south-western Sichuan Basin, China. Geol. J. 56 (7), 3698–3719.
Wei, L., Sun, S., Dong, D., Shi, Z., Yin, J., Zhang, S., Mastalerz, M., Cheng, X., 2021. Petrographic characterization and maceral controls on porosity in overmature marine shales: examples from Ordovician-Silurian shales in China and the US. Geofluids 2021, 5582262.
Wu, Z., He, S., Han, Y., Zhai, G., He, X., Zhou, Z., 2020. Effect of organic matter type and maturity on organic matter pore formation of transitional facies shales: a case study on Upper Permian Longtan and Dalong Shales in middle Yangtze region, China. J. Earth Sci. 31, 368–384.
Xiao, X., Wilkins, R., Liu, D., Liu, Z., Fu, J., 2000. Investigation of thermal maturity of lower Palaeozoic hydrocarbon source rocks by means of vitrinite-like maceral reflectance–a Tarim Basin case study. Org. Geochem. 31, 1041–1052.
Yang, C., Xiong, Y., Zhang, J., 2020. A comprehensive re-understanding of the OM-hosted nanopores in the marine Wufeng–Longmaxi shale formation in South China by organic petrology, gas adsorption, and X-ray diffraction studies. Int. J. Coal Geol. 218, 103362.
Zhang, W., Hu, W., Borjigin, T., Zhu, F., 2020a. Pore characteristics of different organic matter in black shale: a case study of the Wufeng-Longmaxi Formation in the Southeast Sichuan Basin, China. Mar. Pet. Geol. 111, 33–43.
Zhang, Y., He, Z., Lu, S., Jiang, S., Xiao, D., Long, S., Gao, B., Du, W., Zhao, J., Chen, G., Li, Y., 2020b. Characteristics of microorganisms and origin of organic matter in Wufeng Formation and Longmaxi Formation in Sichuan Basin, South China. Mar. Pet. Geol. 111, 363–374.
Zou, C., Qiu, Z., 2021. New advances in unconventional petroleum sedimentology in China. Acta Sedimentol. Sin. 39, 1–9 (in Chinese with English abstract).
Zou, C., Qiu, Z., Poulton, S.W., Dong, D., Wang, H., Chen, D., Lu, B., Shi, Z., Tao, H., 2018. Ocean euxinia and climate change “double whammy” drove the Late Ordovician mass extinction. Geology 46, 535–538.
Zou, C., Zhu, R., Chen, Z., Ogg, J.G., Wu, S., Dong, D., Qiu, Z., Wang, Y., Wang, L., Lin, S., Cui, J., Su, L., Yang, Z., 2019. Organic-matter-rich shales of China. Earth Sci. Rev. 189, 51–78.
Ryder, R.T., Hackley, P.C., Alimi, H., Trippi, M.H., 2013. Evaluation of Thermal Maturity in the Low Maturity Devonian Shales of the Northern Appalachian Basin. AAPG Eastern Section Meeting, AAPG Search and Discovery, Kalamazoo, Michigan, USA, 10477.